# Isotropic-polar phase transitions in an amphiphilic fluid: Density functional theory versus computer simulations

Stefano Giura,[1] Bence G. Márkus,[2] Sabine H. L. Klapp,[3] and Martin Schoen[1,4,*]

[1]*Stranski-Laboratorium für Physikalische und Theoretische Chemie, Fakultät für Mathematik und Naturwissenschaften, Technische Universität Berlin, Straße des 17. Juni 115, Berlin 10623, Germany*

[2]*Institute of Physics, Eötvös University, Pázmány Péter sétány 1/A, H-1117, Hungary*

[3]*Institut für Theoretische Physik, Fakultät für Mathematik und Naturwissenschaften, Technische Universität Berlin, Hardenbergstrasse 36, Berlin 10623, Germany*

[4]*Department of Chemical and Biomolecular Engineering, Engineering Building I, Box 7905, North Carolina State University, 911 Partners Way, Raleigh, North Carolina 27695, USA*

(Received 7 December 2012; published 31 January 2013)

We investigate the critical line separating isotropic from polar phases in an amphiphilic bulk fluid by means of density functional theory (DFT) and Monte Carlo (MC) simulations in the isothermal-isobaric ensemble. The intermolecular interactions are described by a Lennard-Jones potential in which the attractive contribution is modified by an orientation-dependent function. The latter consists of two terms: The first one has the orientation dependence of a classical three-dimensional Heisenberg interaction, whereas, the second one has the orientation dependence of a classical dipole-dipole interaction. However, both contributions are short range. Employing DFT together with a modified mean-field (MMF) approximation for the orientation-dependent pair correlation function, we derive an analytical expression for the critical line separating isotropic from polar liquidlike phases. In parallel MC simulations, we locate the line of critical points through an analysis of Binder's second-order cumulant of the polar-order parameter. Comparison with DFT shows that the dipolelike contribution is irrelevant for the isotropic-polar phase transition. As far as the Heisenberg contribution is concerned, the MC data are in semiquantitative agreement with the DFT predictions for sufficiently strong coupling between molecular orientations. For weaker coupling, the variation in the ratio of critical density and temperature $\rho_c/T_c$ with the Heisenberg coupling constant $\varepsilon_H$ is underestimated by the MMF treatment. The MC results suggest that this is because $\rho_c$ increases with decreasing $\varepsilon_H$ such that the assumption on which the MMF approach rests becomes less applicable in the weaker-coupling limit.

DOI: 10.1103/PhysRevE.87.012313 PACS number(s): 61.25.Em, 05.20.Jj, 64.60.A−, 64.60.fd

## I. INTRODUCTION

To study structure and phase behavior of amphiphilic molecules, Erdmann *et al.* suggested a simple model, involving spherical particles with an internal degree of freedom, a classical "spin" [1]. The particles interact via the well-known Lennard-Jones potential in which the attractive term is properly modified to account for the orientation dependence of the interaction between a pair of amphiphiles. The anisotropic part of the potential introduced by these authors consists of two contributions. The first one describes the orientation dependence of the intermolecular interactions in a classical three-dimensional (3D) Heisenberg fluid (coupling constant $\varepsilon_H$); the other one resembles that of the interactions between a pair of point dipoles (coupling constant $\varepsilon_D$). However, for fixed molecular orientations, both contributions are short range and decay in proportion to $r^{-6}$, where $r$ denotes the distance between the centers of mass of a pair of molecules. For $\varepsilon_H > 0$ and $\varepsilon_D < 0$, the model is capable of producing micellar and lamellar phases characteristic of amphiphilic molecules [2].

For sufficiently large absolute values of $\varepsilon_H$ and $\varepsilon_D$, the amphiphilic fluid exhibits a bulk phase characterized by long-range ordering of the spins [1,3,4]. In a previous paper, we investigated the isotropic-polar (IP) phase transition by means of Monte Carlo (MC) simulations in the isothermal-isobaric ensemble and within the framework of Landau's mean-field theory [3]. The MC simulations are analyzed by applying finite-size scaling theory based upon Binder's second-order cumulant. The two main observations made in this earlier paper are that the IP phase transition is continuous over the range of thermodynamic states considered and that a critical line exists similar to the Curie line in ferroelectrics despite the short-range character of our model potential [3].

In a later paper [4], we determined the critical exponents governing the IP phase transition from which we concluded that our model pertains to the universality class of the classical 3D Heisenberg fluid similar to what has been observed for hard spheres with true (i.e., long-range) dipolar interactions [5,6]. This conclusion is based upon a comparison of the critical exponents $\beta$, $\gamma$, and $\nu$ with data published earlier by Camposstrini *et al.* [7].

However, in view of the fact that our model potential consists of superimposed Heisenberg and dipolar terms, it is not immediately clear what is the respective role of both contributions in the formation of polar phases. For models containing either one of the two separately, IP phase transitions have been investigated in a number of previous papers.

For example, Ayton *et al.* have studied ferroelectric and dipolar glass phases in randomly frozen and dynamically disordered dipolar soft-sphere systems [8,9]. Dipolar fluids with a hard-core prolate or oblate ellipsoidal shape have

*Corresponding author: martin.schoen@tu-berlin.de

 

been studied by Perera and Patey using the hypernetted chain closure in conjunction with density functional theory (DFT) [10]. A little later, Wei and Patey investigated a system of strongly dipolar soft spheres by mean of molecular dynamics simulations [11–13]. For the first time, these authors could demonstrate that dipolar forces alone can lead to the formation of a ferroelectric nematic phase.

A large body of work on fluids with electrostatic point dipoles has been published by Dietrich and co-workers. Frodl and Dietrich [14,15] developed a DFT scheme, giving results that are in reasonable qualitative agreement with MC data. Later, Groh and Dietrich studied the formation of ferroelectric phases in Stockmayer fluids by means of DFT [16]. These authors demonstrated that, in the polar phase, the free-energy density depends crucially on the shape of the domain under consideration as well as on the dielectric permittivity of the surroundings. In a later paper, the same authors extended their earlier work to account for the formation of ferromagnetic solids [17], included external fields [18,19], and considered particles with a nonspherical hard core [20].

Klapp and co-workers investigated the isotropic-ferroelectric phase transition of dipolar hard spheres via various integral-equation approaches and a related DFT [21,22]. In particular, they demonstrated the possibility of a suppression of the ferroelectric fluid phase by a ferroelectric solid [23,24]. Later, Range and Klapp [25] applied the modified mean-field (MMF) DFT approach introduced and developed earlier [14–16,26] to study the phase behavior of binary hard-sphere mixtures with embedded electrostatic point dipoles. An application to confined pure dipolar fluids has been considered by Klapp and co-workers based upon integral-equation approaches [27] and DFT [28].

By means of MC simulations Tavares *et al.* investigated the structure of a two-dimensional hard-disk fluid with an embedded point dipole [29]. These authors analyzed the topology of clusters forming in the fluid at low and intermediate densities and observed that the structure of the fluid can be well described by an ideal mixture of such clusters arising from a self-assembly mechanism.

Compared with fluids in which the orientation dependence of the intermolecular interactions is described by that between point dipoles, less attention has been devoted to the phase behavior of Heisenberg fluids [7,26,30–40]. Of these earlier papers, several are of particular importance. Both Tavares *et al.* [26] and Weis *et al.* [38] demonstrate that, in a ferromagnetic Heisenberg fluid, the Curie line, separating isotropic from polar phases, may either end in a tricritical point or terminate at a critical end point depending on the relative strengths of the radial parts of the isotropic and the anisotropic contributions to the overall intermolecular interaction potentials. For a ferromagnetic Heisenberg fluid with Yukawa shielding, Lomba *et al.* preclude the existence of a tricritical point in which the Curie line ends [36]. Based upon their combined simulation and integral-equation approaches, these authors suggest a termination of the Curie line in a critical end point instead. For the sake of conciseness of the present paper, we defer a more detailed investigation of the existence of a tricritical point in our particular model to a separate paper. Lomba *et al.* also considered the antiferromagnetic Heisenberg fluid where the formation of ordered states is signaled by an increase in the nematic rather than the polar-order parameter.

The remainder of our paper is organized as follows. In Sec. II, we introduce the model potential for our amphiphilic fluid. Section III is given to a discussion of the DFT theory on which our theoretical work is based. Concepts of finite-size scaling are introduced in Sec. IV. Results from MC and a comparison with the DFT predictions are presented in Sec. V. The paper concludes with a summary of our main findings in Sec. VI.

## II. MODEL

In this paper, we consider a bulk fluid composed of $N$ amphiphilic molecules interacting with each other in a pairwise additive fashion. Hence, we express the total configurational potential energy as

$$\Phi(\boldsymbol{R},\boldsymbol{\Omega}) = \frac{1}{2}\sum_{i=1}^{N}\sum_{\substack{j=1\\ j\neq i}}^{N}\varphi(\boldsymbol{r}_{ij},\omega_i,\omega_j). \tag{2.1}$$

In Eq. (2.1), $\boldsymbol{r}_{ij} = \boldsymbol{r}_i - \boldsymbol{r}_j$ is the distance vector between the centers of mass of molecules $i$ and $j$ located at $\boldsymbol{r}_i$ and $\boldsymbol{r}_j$, respectively. We also introduce shorthand notations for the sets of center-of-mass positions $\boldsymbol{R} \equiv \{\boldsymbol{r}_1,\boldsymbol{r}_2,\ldots,\boldsymbol{r}_N\}$ and the set of polar angles $\boldsymbol{\Omega} \equiv \{\omega_1,\omega_2,\ldots,\omega_N\}$, specifying the orientations of the $N$ amphiphiles where $\omega_i \equiv (\vartheta_i,\varphi_i)$ for a system of molecules of uniaxial symmetry and $\vartheta_i$ and $\varphi_i$ are the associated Euler angles. In Eq. (2.1), the intermolecular interaction potential $\varphi$ can be split into an isotropic and an anisotropic contribution according to

$$\varphi(\boldsymbol{r}_{ij},\omega_i,\omega_j) = \varphi_{\rm iso}(r_{ij}) + \varphi_{\rm anis}(\boldsymbol{r}_{ij},\omega_i,\omega_j), \tag{2.2}$$

where $r_{ij} = |\boldsymbol{r}_{ij}|$. In Eq. (2.2), $\varphi_{\rm iso}$ is given by the standard Lennard-Jones potential function,

$$\begin{aligned}\varphi_{\rm iso}(r_{ij}) &= 4\varepsilon\left[\left(\frac{\sigma}{r_{ij}}\right)^{12} - \left(\frac{\sigma}{r_{ij}}\right)^{6}\right]\\ &\equiv \varphi_{\rm rep}(r_{ij}) + \varphi_{\rm att}(r_{ij}),\end{aligned} \tag{2.3}$$

where $\varphi_{\rm rep}$ and $\varphi_{\rm att}$ denote repulsive and attractive contributions to $\varphi_{\rm iso}$, respectively. From Eq. (2.3), we see that our amphiphilic molecules are approximately spherical with $\sigma$ being the "diameter" and $\varepsilon$ being the depth of the attractive well. The anisotropic contribution to $\varphi$ is modeled according to

$$\varphi_{\rm anis}(\boldsymbol{r}_{ij},\omega_i,\omega_j) = \varphi_{\rm att}(r_{ij})\Psi(\widehat{\boldsymbol{r}}_{ij},\omega_i,\omega_j), \tag{2.4}$$

and, therefore, has the same distance dependence as the attractive part of the isotropic interaction potential. Hence, both $\varphi_{\rm iso}$ and $\varphi_{\rm anis}$ are short range.

The function $\Psi$ in Eq. (2.4) describes the anisotropy of the intermolecular interactions and is given by

$$\begin{aligned}\Psi(\widehat{\boldsymbol{r}}_{ij},\omega_i,\omega_j) \equiv{}& 3\,\varepsilon_{\rm H}\widehat{\boldsymbol{u}}(\omega_i)\cdot\widehat{\boldsymbol{u}}(\omega_j)\\ &+\sqrt{\frac{15}{2}}\varepsilon_{\rm D}\{3[\widehat{\boldsymbol{u}}(\omega_i)\cdot\widehat{\boldsymbol{r}}_{ij}][\widehat{\boldsymbol{u}}(\omega_j)\cdot\widehat{\boldsymbol{r}}_{ij}]\\ &-\widehat{\boldsymbol{u}}(\omega_i)\cdot\widehat{\boldsymbol{u}}(\omega_j)\},\end{aligned} \tag{2.5}$$

following an original suggestion by Erdmann *et al.* [1]. Here and below, the notation "$\widehat{\cdots}$" is used for unit vectors where,

in particular, $\widehat{\boldsymbol{r}}_{ij} = \boldsymbol{r}_{ij}/r_{ij}$. From Eq. (2.5), one realizes that the orientation dependence of the interaction consists of a contribution characteristic of a classical 3D Heisenberg fluid [41] with coupling constant $\varepsilon_{\rm H}$ and a second contribution that is analogous to the orientation dependence of the interaction between electrostatic point dipoles with coupling constant $\varepsilon_{\rm D}$ [42]. Specifically, because $\varphi_{\rm att} < 0$, the choice $\varepsilon_{\rm D} > 0$ corresponds to a short-range version of the classical dipole-dipole potential. Therefore, $\varepsilon_{\rm D}$ plays a role similar to the squared dipole moment $\mu^2$ that arises in the (electrostatic or magnetic) dipole-dipole interaction potential.

The subsequent treatment will greatly benefit from rewriting Eq. (2.5) in terms of rotational invariants (see Appendix A of Ref. [43]). Rotational invariants are defined as

$$\Phi_{l_i l_j l}(\omega_i,\omega_j,\omega) \equiv \sum_{m_i m_j m} C(l_i l_j l; m_i m_j m) Y_{l_i m_i}(\omega_i) Y_{l_j m_j}(\omega_j) Y^*_{lm}(\omega), \quad (2.6)$$

where $C$ is a Clebsch-Gordan coefficient, $Y$ is a spherical harmonic, and the superscript "*" denotes the complex conjugate. The solid angle $\omega$ describes the orientation of $\widehat{\boldsymbol{r}}_{ij}$ in a space-fixed frame of reference and the integer $m_i \in \{-l_i,\ldots,l_i\}$. This relation is also satisfied by the pairs $(l_j,m_j)$ and $(l,m)$. The Clebsch-Gordan coefficient vanishes unless $m = m_i + m_j$ and $|l_i - l_j| \leqslant l \leqslant l_i + l_j$ (see Eqs. (A.130) and (A.131) of Ref. [43]). Using these properties, one finds (see pp. 496–497 of Ref. [43])

$$\Phi_{110} = -(4\pi)^{-3/2}\sqrt{3}\widehat{\boldsymbol{u}}(\omega_i)\cdot\widehat{\boldsymbol{u}}(\omega_j), \quad (2.7a)$$

$$\Phi_{112} = -(4\pi)^{-3/2}\sqrt{\frac{15}{2}}\{3[\widehat{\boldsymbol{u}}(\omega_i)\cdot\widehat{\boldsymbol{r}}_{ij}][\widehat{\boldsymbol{u}}(\omega_j)\cdot\widehat{\boldsymbol{r}}_{ij}] - \widehat{\boldsymbol{u}}(\omega_i)\cdot\widehat{\boldsymbol{u}}(\omega_j)\}, \quad (2.7b)$$

where the arguments $\omega_i$, $\omega_j$, and $\omega$ of the spherical invariants are dropped for notational convenience. With the expressions given in Eqs. (2.7), it is now easy to verify that the anisotropy function in Eq. (2.5) can then be recast compactly as

$$\Psi(\widehat{\boldsymbol{r}}_{ij},\omega_i,\omega_j) = -(4\pi)^{3/2}(\sqrt{3}\varepsilon_{\rm H}\Phi_{110} + \varepsilon_{\rm D}\Phi_{112}). \quad (2.8)$$

Notice that, from Eqs. (2.3), (2.4), (2.7b), and (2.8), it is evident that the orientation dependence of the second term in parentheses on the right side of Eq. (2.8) is the same as that of the potential describing the interaction between a pair of classical point dipoles as long as $\varepsilon_{\rm D} > 0$.

## III. DENSITY FUNCTIONAL THEORY

For the model fluid introduced in Sec. II, we now derive an explicit expression for the line of critical points at which the amphiphilic fluid undergoes an IP phase transition [3]. This analysis will be based on a MMF treatment of the free energy of our model fluid. To that end, we will develop an explicit expression for the excess free energy in the subsequent Sec. III A, which we will then use in a Landau expansion to locate the line of critical points in Sec. III B. The resulting expressions can be evaluated within the framework of a high-temperature expansion of the orientation-dependent Mayer $f$ function (see Sec. III C), which arises on account of the modified mean-field approximation introduced in Sec. III A. Consequences of the approach to be developed in Secs. III A–III C are discussed in Sec. III D.

### A. Modified mean-field theory

Our point of departure is the expression,

$$\Delta\mathcal{F}^{\rm ex} = \frac{1}{2}\int_0^1 d\lambda \int d\boldsymbol{r}_1 d\boldsymbol{r}_2 \int d\omega_1 d\omega_2 \rho(\boldsymbol{r}_1,\omega_1)\rho(\boldsymbol{r}_2,\omega_2) \times g(\boldsymbol{r}_{12},\omega_1,\omega_2;\lambda)\frac{\partial}{\partial\lambda}[\varphi_{\rm hs}(r_{12}t) + \lambda\varphi(\boldsymbol{r}_{12},\omega_1,\omega_2)] \quad (3.1)$$

for the change in the interaction (excess) part of the free energy caused by the perturbation $\varphi(\boldsymbol{r}_{12},\omega_1,\omega_2)$ [see Eq. (2.2)] *relative* to the excess free energy of a hard-sphere reference system. Equation (3.1) is exact for systems with pairwise additive intermolecular interactions and was originally developed some time ago by Evans [44]. In Eq. (3.1),

$$\varphi_{\rm hs}(r_{12}) = \begin{cases} \infty, & r_{12} < \sigma, \\ 0, & r_{12} \geqslant \sigma \end{cases} \quad (3.2)$$

is the interaction potential between hard spheres of diameter $\sigma$, $\rho(\boldsymbol{r}_k,\omega_k)$ is the orientation-dependent local density of particle $k$ ($k = 1,2$), and $g(\boldsymbol{r}_{12},\omega_1,\omega_2;\lambda)$ is the pair correlation function. The hard-sphere fluid is chosen here for two reasons. First, it is computationally convenient in that it helps to simplify the integrations over $d\boldsymbol{r}_1$ and $d\boldsymbol{r}_2$ later on. Second, the precise physical nature of the reference system is irrelevant for the primary goal of this paper, namely, to determine the critical line of IP phase transition. The latter aspect will become apparent in Sec. III B below. The dimensionless parameter $\lambda$ is introduced to take us from the reference system to the system of interest in which the intermolecular interactions are described by the potential function $\varphi(\boldsymbol{r}_{12},\omega_1,\omega_2)$ introduced in Eq. (2.2).

Following earlier papers [14–16,25,28,45], we approximate the pair correlation function in Eq. (3.1) by the expression,

$$g(\boldsymbol{r}_{12},\omega_1,\omega_2;\lambda) = \begin{cases} 0, & r_{12} \leqslant \sigma, \\ \exp[-\beta_{\rm B}(\varphi_{\rm hs} + \lambda\varphi)], & r_{12} \geqslant \sigma. \end{cases} \quad (3.3)$$

The expression on the second line of Eq. (3.3) is exact in the limit of vanishing number density regardless of temperature $T$. In Eq. (3.3), $\beta_{\rm B} \equiv 1/k_{\rm B}T$, where $k_{\rm B}$ denotes Boltzmann's constant. Performing, in Eq. (3.1), the differentiation with respect to $\lambda$ and using the approximation Eq. (3.3), one may carry out the integration over $d\lambda$ in Eq. (3.1) analytically to obtain

$$\begin{aligned}\beta_{\rm B}\Delta\mathcal{F}^{\rm ex} &= -\frac{1}{2}\int d\boldsymbol{r}_1 d\boldsymbol{r}_2 \int d\omega_1 d\omega_2 \rho(\boldsymbol{r}_1,\omega_1)\rho(\boldsymbol{r}_2,\omega_2) \\ &\quad\times \exp[-\beta_{\rm B}\varphi_{\rm hs}(r_{12})] f(\boldsymbol{r}_{12},\omega_1,\omega_2) \\ &= -\frac{1}{2}\int_{r_{12}\geqslant\sigma} d\boldsymbol{r}_1 d\boldsymbol{r}_2 \int d\omega_1 d\omega_2 \rho(\boldsymbol{r}_1,\omega_1)\rho(\boldsymbol{r}_2,\omega_2) \\ &\quad\times f(\boldsymbol{r}_{12},\omega_1,\omega_2), \end{aligned} \quad (3.4)$$

where

$$f(\boldsymbol{r}_{12},\omega_1,\omega_2) \equiv \exp[-\beta_B\varphi(\boldsymbol{r}_{12},\omega_1,\omega_2)] - 1 = \exp[-\beta_B\varphi_{iso}(r_{12})] \times \exp[-\beta_B\varphi_{anis}(\boldsymbol{r}_{12},\omega_1,\omega_2)] - 1 \quad (3.5)$$

is the orientation-dependent Mayer $f$ function [43].

In this paper, we are concerned exclusively with bulk phases characterized by a uniform number density. Hence, we may factorize the local densities in Eq. (3.4) according to

$$\rho(\boldsymbol{r},\omega) = \rho\alpha(\omega), \quad (3.6)$$

where the orientational distribution function is normalized such that it satisfies

$$\int d\omega\, \alpha(\omega) = 1. \quad (3.7)$$

In the isotropic phase where $\alpha(\omega)$ is constant, the normalization condition implies $\alpha(\omega) = 1/4\pi$ reflecting full rotational symmetry. In the polar phase, there is still cylindrical symmetry with respect to the so-called director, that is, the average orientation of the particles' spins. We, therefore, follow Range and Klapp [25] who expanded the orientational distribution function in terms of Legendre polynomials $\{P_L\}$ via

$$2\pi\alpha(\omega) \equiv \overline{\alpha}(\cos\,\theta) = \frac{1}{2} + \sum_{L=1}^{\infty}\alpha_L P_L(\cos\,\theta), \quad (3.8)$$

where $\alpha_0 = \frac{1}{2}$ for the isotropic phase is treated separately such that Eq. (3.8) is consistent with Eq. (3.7). Members of the set of expansion coefficients $\{\alpha_L\}_{L\geqslant 1}$ are related to order parameters characterizing the polar state [16,25]. Using the definition of the spherical harmonics (see Eqs. (A.2) and (A.4) of Ref. [43]), one has the relation,

$$P_L(\cos\,\theta) = \sqrt{\frac{4\pi}{2L+1}}Y_{L0}(\omega). \quad (3.9)$$

Now, employing Eqs. (3.6), (3.8), and (3.9), one can rewrite Eq. (3.4) as

$$\frac{\beta_B\Delta\mathcal{F}^{ex}}{V} = -\frac{1}{2}\left(\frac{\rho}{2\pi}\right)^2\sum_{L_1=0}^{\infty}\sum_{L_2=0}^{\infty}\sqrt{\frac{(4\pi)^2}{(2L_1+1)(2L_2+1)}}\alpha_{L_1}\alpha_{L_2} \times \int_{r_{12}\geqslant\sigma} d\boldsymbol{r}_{12}\int d\omega_1 d\omega_2 Y_{L_10}(\omega_1)Y_{L_20}(\omega_2)f(\boldsymbol{r}_{12},\omega_1,\omega_2). \quad (3.10)$$

Next we notice that, by analogy with Eq. (3.143) of Ref. [43], the Mayer $f$ function can be expressed in terms of rotational invariants according to

$$f(\boldsymbol{r}_{12},\omega_1,\omega_2) = \sum_{l_1l_2l} f_{l_1l_2l}(r_{12})\Phi_{l_1l_2l}(\omega_1,\omega_2,\omega), \quad (3.11)$$

where $\{f_{l_1l_2l}(r_{12})\}$ are expansion coefficients that depend only on the distance $r_{12}$ between particles of the molecular pair. From the definition of the rotational invariants given in Eq. (2.6), it follows that the set $\{\Phi_{l_1l_2l}\}$ satisfies the orthogonality relation [16],

$$\int d\omega_1 d\omega_2 d\omega\, \Phi_\Lambda(\omega_1,\omega_2,\omega)\Phi^*_{\Lambda'}(\omega_1,\omega_2,\omega) = \frac{2l+1}{4\pi}\delta_{\Lambda\Lambda'}, \quad (3.12)$$

where the sets $\Lambda = \{l_1l_2l\}$ and $\Lambda' = \{l_1'l_2'l'\}$. Hence, from Eq. (3.11), one can obtain the expansion coefficients $f_{l_1l_2l}(r_{12})$ via

$$f_{l_1l_2l}(r_{12}) = \frac{4\pi}{2l+1}\int d\omega_1 d\omega_2 d\omega\, f(\boldsymbol{r}_{12},\omega_1,\omega_2)\Phi^*_{l_1l_2l}(\omega_1,\omega_2,\omega). \quad (3.13)$$

Inserting Eq. (3.11) into Eq. (3.10) and changing to spherical coordinates (i.e., $d\boldsymbol{r}_{12} \to r_{12}^2 dr_{12}d\omega$), one obtains

$$\frac{\beta_B\Delta\mathcal{F}^{ex}}{V} = -\frac{1}{2}\left(\frac{\rho}{2\pi}\right)^2\sum_{L_1=0}^{\infty}\sum_{L_2=0}^{\infty}\sqrt{\frac{(4\pi)^2}{(2L_1+1)(2L_2+1)}}\alpha_{L_1}\alpha_{L_2} \times \sum_{l_1l_2l}\int dr_{12}r_{12}^2 f_{l_1l_2l}(r_{12})\int d\omega_1 d\omega_2 d\omega \times Y_{L_10}(\omega_1)Y_{L_20}(\omega_2)\Phi_{l_1l_2l}(\omega_1,\omega_2,\omega). \quad (3.14)$$

Using the definition of rotational invariants given in Eq. (2.6), one notices that the integration over $d\omega$ involves only the spherical harmonics $Y_{lm}$ of $\Phi_{l_1l_2l}$. Therefore, the integral vanishes except when $l = m = 0$ as a consequence of Eq. (A.38) of Ref. [43].

Moreover, the Clebsch-Gordan coefficients vanish unless the triangle relation $|l_1 - l_2| \leqslant l \leqslant l_1 + l_2$ is satisfied. Combining this with the condition $l = 0$ implies that the integration over orientations in Eq. (3.14) is nonzero only when $l_1 = l_2 = L$ such that the triple sum over $l_1$, $l_2$, and $l$ reduces to a single one, that is,

$$\frac{\beta_B\Delta\mathcal{F}^{ex}}{V} = -\frac{1}{2}\left(\frac{\rho}{2\pi}\right)^2\sum_{L_1=0}^{\infty}\sum_{L_2=0}^{\infty}\sqrt{\frac{(4\pi)^2}{(2L_1+1)(2L_2+1)}} \times \alpha_{L_1}\alpha_{L_2}\sum_{L=0}^{\infty}\int dr_{12}r_{12}^2 f_{LL0}(r_{12}) \times \int d\omega_1 d\omega_2 d\omega\, Y_{L_10}(\omega_1)Y_{L_20}(\omega_2) \times \Phi_{LL0}(\omega_1,\omega_2,\omega). \quad (3.15)$$

In addition, the integration over $d\omega_i$ $(i = 1,2)$ involves products of spherical harmonics of the form $Y_{L_10}(\omega_1)Y_{Lm_1}(\omega_1)$ and $Y_{L_20}(\omega_2)Y_{Lm_2}(\omega_2)$ such that the corresponding integrals in Eq. (3.15) vanish because of the orthogonality of the spherical harmonics (see, for example, Eq. (A39) of Ref. [43]) unless $L_1 = L_2 = L$ and $m_1 = m_2 = 0$. Consequently, the only nonvanishing Clebsch-Gordan coefficients in the expansion Eq. (3.11) are $(L \to l)$,

$$C(ll0;000) = \frac{(-1)^l}{\sqrt{2l+1}}. \quad (3.16)$$

Putting all this together, one eventually realizes that Eq. (3.10) is recast compactly as

$$\frac{\beta_B \Delta\mathcal{F}^{ex}}{V} = \rho^2 \sum_{l=0}^{\infty} \alpha_l^2 u_l, \tag{3.17}$$

where $u_l$ is given by

$$u_l = -\frac{(-1)^l}{\sqrt{\pi}(2l+1)^{3/2}} \int_\sigma^\infty dr_{12} r_{12}^2 f_{ll0}(r_{12}). \tag{3.18}$$

Together, Eqs. (3.17) and (3.18) constitute the MMF treatment of the excess free energy of our model fluid.

Finally, the total free energy of our system may be cast as [25]

$$\mathcal{F} = \mathcal{F}^{hs} + \mathcal{F}^{id} + \Delta\mathcal{F}^{ex}, \tag{3.19}$$

where the ideal-gas contribution may be expressed as

$$\frac{\beta_B \mathcal{F}^{id}}{V} = \rho[\ln(\rho\Lambda^5 \mathcal{M}/\mathcal{I}) - 1] + \rho \int_{-1}^{1} dx\, \overline{\alpha}(x) \ln[2\overline{\alpha}(x)]. \tag{3.20}$$

In Eq. (3.20), $x \equiv \cos\theta$, $\mathcal{M}$ stands for the molecular mass, $\mathcal{I}$ stands for the moment of inertia of an amphiphile, $\Lambda \equiv \sqrt{\beta_B h^2/2\pi\mathcal{M}}$ is the thermal de Broglie wavelength, and the exponent 5 accounts for the three translational and two rotational degrees of freedom. However, as we argue in the subsequent Sec. III B, the first summand on the right side of Eq. (3.20) is irrelevant in locating the critical line of IP phase transitions.

The second summand on the right side of Eq. (3.20) represents the loss of rotational entropy our fluid suffers upon entering the polar (i.e., ordered) phase. Notice that, in the argument of the logarithm on the right side of Eq. (3.20), we have arbitrarily introduced an additional factor of 2 that causes the integral to vanish in the isotropic phase because of the definition of $\overline{\alpha}(x)$ in Eq. (3.8). The deliberate factor of 2 changes the free energy only by a constant, which is irrelevant because we are interested only in *changes* in free energy henceforth.

For the free energy of the hard-sphere reference system, one could employ the well-known Carnahan-Starling expression [46]. However, like the first summand on the right side of Eq. (3.20), the precise form of $\mathcal{F}^{hs}$ is irrelevant for the determination of the critical line of IP phase transitions.

### B. The critical line

To proceed, it is convenient to follow Range and Klapp [25] by introducing

$$\frac{\beta_B \Delta\mathcal{F}}{V} \equiv \frac{\beta_B \mathcal{F}}{V} - \frac{\beta_B \mathcal{F}^{hs}}{V} - \rho[\ln(\rho\Lambda^5\mathcal{M}/\mathcal{I}) - 1] - \frac{\rho^2}{4} u_0 = \rho \int_{-1}^{1} dx\, \overline{\alpha}(x) \ln[2\overline{\alpha}(x)] + \rho^2 \sum_{l=1}^{\infty} \alpha_l^2 u_l, \tag{3.21}$$

which is zero in the isotropic phase where $\overline{\alpha}(x) = \frac{1}{2}$ [see Eq. (3.8)], and the set of order parameters $\{\alpha_l\}_{l\geqslant 1}$ vanishes identically. Consequently, any nonzero value of $\Delta\mathcal{F}$ signals the onset of order in the amphiphilic fluid. To determine the critical line $\rho_c(T_c)$, we need to locate thermodynamic state points at which $\Delta\mathcal{F}$ deviates from zero. To that end, we follow Groh and Dietrich [16] who showed, for a system of electrostatic point dipoles, that the leading contribution to $\Delta\mathcal{F}$ due to intermolecular interactions is given by the term $l = 1$ in the sum on the right side of Eq. (3.21). Similar conclusions have been drawn by Range and Klapp for binary mixtures of electrostatic point dipoles [25].

The expression in Eq. (3.21) can be simplified further by realizing that, at the onset of the IP phase transition, the deviation in the set of expansion coefficients $\{\alpha_l\}$ from zero will be small. Hence, using, in Eq. (3.21), $\xi \equiv \sum_{l=1} \alpha_l P_l(x)$ and expanding the integrand on the right side in a Taylor series, one obtains [25]

$$\left(\frac{1}{2} + \xi\right) \ln(1 + 2\xi) = \xi + \xi^2 + \cdots. \tag{3.22}$$

In addition, using the fact that $\int_{-1}^{1} dx\, P_l(x) = 0$ for $l \geqslant 1$ and the orthogonality of Legendre polynomials (see, for example, Eq. (A9.b) of Ref. [43]), we conclude that

$$\int_{-1}^{1} dx\, \overline{\alpha}(x) \ln[2\overline{\alpha}(x)] = \sum_{l=1}^{\infty} \left(\frac{2}{2l+1}\right) \alpha_l^2 + \cdots, \tag{3.23}$$

so that Eq. (3.21) can be rewritten as

$$\frac{\beta_B \Delta\mathcal{F}}{V} = \sum_{l=1}^{\infty} \left(\frac{2}{2l+1}\rho + u_l \rho^2\right) \alpha_l^2. \tag{3.24}$$

Concentrating on the leading term in Eq. (3.24), we arrive at the approximate formula,

$$\frac{\beta_B \Delta\mathcal{F}}{V} \simeq \rho\left(\frac{2}{3} + \rho u_1\right) \alpha_1^2 = 0, \tag{3.25}$$

as the constitutive equation from which the critical density along the line of IP phase transitions can be obtained. As long as the expression in Eq. (3.25) vanishes, the isotropic phase is thermodynamically stable. Clearly, besides the trivial and physically uninteresting solution $\rho_c = 0$, Eq. (3.25) leads to the simple formula,

$$\rho_c = -\frac{2}{3}\frac{1}{u_1}, \tag{3.26}$$

which is in complete agreement with Eq. (7.10) of Groh and Dietrich [16] and Eq. (2.37) of Range and Klapp [25].

### C. High-temperature expansion of the Mayer $f$ function

In Eq. (3.26),

$$u_1 = \frac{1}{3\sqrt{3\pi}} \int_\sigma^\infty dr_{12} r_{12}^2 f_{110}(r_{12}), \tag{3.27}$$

and

$$f_{110}(r_{12}) = 4\pi \int d\omega_1 d\omega_2 d\omega\, f(\boldsymbol{r}_{12}, \omega_1, \omega_2) \Phi_{110}(\omega_1, \omega_2, \omega) \tag{3.28}$$

are special cases of the general expressions given in Eqs. (3.13) and (3.18) where we also used the fact that $\Phi_{110} = \Phi_{110}^*$.

To proceed, we approximate the Mayer $f$ function by assuming that, at the onset of the formation of a polar phase, $\beta_B \varphi_{anis} \ll 1$ [see Eq. (2.4)]. Hence, we expand $\exp[-\beta_B \varphi_{anis}]$

TABLE I. Values of the integral $\mathcal{I}_{pq}$ [see Eq. (3.30)] for various combinations of the integers $p$ and $q$. The sum $p+q$ refers to the order of terms in the expansion of the Mayer $f$ function [see Eq. (3.29)], which is identified through entries in the last column of the table.

| $p$ | $q$ | $p+q$ | $\mathcal{I}_{pq}$ | Order |
|---|---|---|---|---|
| 1 | 0 | 1 | 0 | Zeroth |
| 2 | 0 | 2 | $\frac{1}{4\pi}$ | First |
| 1 | 1 | 2 | 0 | |
| 3 | 0 | 3 | 0 | Second |
| 2 | 1 | 3 | 0 | |
| 1 | 2 | 3 | 0 | |
| 4 | 0 | 4 | $\frac{9}{5}\frac{1}{(4\pi)^4}$ | Third |
| 3 | 1 | 4 | 0 | |
| 2 | 2 | 4 | $\frac{27}{5}\frac{1}{(4\pi)^4}$ | |
| 1 | 3 | 4 | $-9\sqrt{\frac{2}{5}}\frac{1}{(4\pi)^4}$ | |

in a power series which we truncate after the cubic term such that we obtain, from the last line of Eq. (3.5), the approximate expression,

$$f = \exp(-\beta_B\varphi_{iso})\left[1-\beta_B\varphi_{anis}+\frac{(\beta_B\varphi_{anis})^2}{2!}-\frac{(\beta_B\varphi_{anis})^3}{3!}\pm\cdots\right]-1. \quad (3.29)$$

Our motivation to keep terms up to cubic order (rather than truncating the expansion after the second-order term), as has often been performed in other MMF DFT papers [16,45], becomes apparent in the subsequent Sec. III D. Inserting Eq. (3.29) into Eq. (3.28) and using Eqs. (2.4) and (2.8), one realizes that the resulting expression for $f_{110}(r_{12})$ involves integrals of the general form

$$\mathcal{I}_{pq} \equiv \int d\omega_1 d\omega_2 d\omega\, \Phi^p_{110}(\omega_1,\omega_2,\omega)\Phi^q_{112}(\omega_1,\omega_2,\omega), \quad (3.30)$$

where different combinations of $p$ and $q$ arise from the constant, linear, quadratic, and cubic terms in the expansion of $\exp(-\beta_B\varphi_{anis})$ in Eq. (3.29). For the sake of clarity, we list these various integrals in Table I. Applying the product rule for rotational invariants (see, for example, Eq. (B8) of Ref. [16]) to products of powers of $\Phi_{110}$ and $\Phi_{112}$ iteratively, considering that one can express these products in terms of linear combinations of other rotational invariants, and employing the general relation,

$$\int d\omega_1 d\omega_2 d\omega\, \Phi_{l_1 l_2 l} = \begin{cases}\sqrt{4\pi}, & l_1=l_2=l=0,\\ 0, & \text{otherwise},\end{cases} \quad (3.31)$$

entries in Table I are obtained.

After some tedious but otherwise straightforward algebra, from Eq. (3.29), one obtains, with the aid of entries in Table I,

$$f_{110}(r_{12}) = (4\pi)^{3/2}\sqrt{3}\exp[-\beta_B\varphi_{iso}(r_{12})]\times\left\{\beta_B\varphi_{att}(r_{12})\varepsilon_H+\frac{9}{10}[\beta_B\varphi_{att}(r_{12})]^3\times\left(\varepsilon_H^3+3\varepsilon_H\varepsilon_D^2-\frac{1}{3}\sqrt{\frac{10}{3}}\varepsilon_D^3\right)\right\}. \quad (3.32)$$

Inserting Eq. (3.32) into Eq. (3.27), we then finally arrive at

$$u_1 = \frac{8\pi}{3}\left\{\beta_B\mathcal{I}^{(1)}\varepsilon_H+\beta_B^3\mathcal{I}^{(3)}\times\frac{9}{10}\left(\varepsilon_H^3+3\varepsilon_H\varepsilon_D^2-\frac{1}{3}\sqrt{\frac{10}{3}}\varepsilon_D^3\right)\right\}, \quad (3.33)$$

where the integrals,

$$\mathcal{I}^{(n)} \equiv \int_\sigma^\infty dr_{12} r_{12}^2[\varphi_{att}(r_{12})]^n \exp[-\beta_B\varphi_{iso}(r_{12})] \quad (3.34)$$

have to be solved numerically. With the aid of Eqs. (3.33) and (3.34), we compute the line of IP phase transitions from Eq. (3.26).

### D. Consequences

In view of our numerical results presented later in Sec. V, it is instructive to briefly analyze the result given in Eq. (3.33) from a formal point of view. We start by considering the contribution to $u_1$ from the first-order term in the corresponding expansion of the Mayer $f$ function [see Eq. (3.29)]. This contribution depends solely on the coupling constant of the Heisenberg interaction. Specifically, because $\mathcal{I}^{(1)}$ is negative and $\varepsilon_H$ is positive for a ferromagnetic Heisenberg interaction, the entire first-order contribution to $u_1$ is negative and, thus, can generate a positive critical density [see Eq. (3.26)]. We also see (focusing again on the first-order term) that the larger $\epsilon_H$, the larger this first-order contribution becomes. This yields a decrease in $\rho_c$ at fixed inverse temperature $\beta_B$. In other words, an increase in $\varepsilon_H$ supports the IP phase transition as one might expect.

Consider now the third-order contribution which depends on both the Heisenberg and the dipolar contribution (which we assume to be truly dipolarlike in the sense that $\varepsilon_D > 0$). The prefactor of the third-order term to $u_1$, determined by the integral $\mathcal{I}^{(3)}$, is again negative on one hand. On the other hand, the function $f(x) \equiv 1+3x^2-\frac{1}{3}\sqrt{10/3}x^3$, determining the expression in parentheses in Eq. (3.33) with $x \equiv \varepsilon_D/\varepsilon_H$, has a nonmonotonic behavior and can even change sign. Specifically, for $x=0$, that is, in the absence of the dipolelike interaction, we find $f(x)=1>0$, indicating that the third-order contribution for a pure Heisenberg system supports the IP phase transition. The dipolar term even enhances this behavior as long as it is not too large. Indeed, $f(x)$ increases with $x$ towards larger positive values up to a value of $x_{max} \approx 3.4$. For larger coupling ratios $x$, $f(x)$ decreases again and finally becomes even negative. We can, thus, conclude that the impact of $\varepsilon_D$ on the IP phase transition depends strongly on the ratio of the dipolar and Heisenberg coupling constants. Our results, presented in Sec. V, focus mostly on the case of $x=0.5$.

Another interesting point to note is that, in the absence of the Heisenberg contribution, there is no IP phase transition at all. This conclusion is drawn on the basis of the observation that, for $\varepsilon_H=0$, Eq. (3.33) reduces to the expression,

$$u_1 = -\frac{4\pi}{5}\sqrt{\frac{10}{3}}\beta_B^3\mathcal{I}^{(3)}\varepsilon_D^3. \quad (3.35)$$

For $\varepsilon_D > 0$ (which is the choice adopted predominantly in the present paper), it follows that $u_1 > 0$ because $\mathcal{I}^{(3)} < 0$

[see Eqs. (2.4) and (3.34)]. Thus, because $u_1 > 0$, the critical density would turn out to be negative [see Eq. (3.26)], which is unphysical.

On the contrary, an ordered ferroelectric phase forms in fluids in which molecules are carrying an electrostatic (point) dipole [16,25,47]. Whereas, the orientation dependence of the interaction between a pair of electrostatic dipoles is the same as in the dipolar contribution to $\varphi_{\text{anis}}$ of the present model system, the range of the interactions is different. Therefore, it seems sensible to ascribe the absence of an IP phase transition in our model fluid in the case of $\varepsilon_{\text{H}} = 0$ to the short-range nature of $\varphi_{\text{anis}}$. We note that the role of the long-range nature of the dipolar interactions for the existence of a ferroelectric transition has also been pointed out in previous theoretical papers on the basis of free-energy arguments [9,13,48] and integral-equation methods [13,21]. In these approaches, the long-range nature enters via a shape (or boundary-condition) dependence of the free energy of the homogeneous system [9,13,48] and a nonvanishing of certain coefficients of the direct correlation function [13,21]. This leads to a divergence of the dielectric constant when the dense isotropic liquid is cooled down. All these approaches would fail to predict a ferroelectric phase if the dipolar interaction were short ranged.

By a similar token, an IP phase transition cannot take place if $\varepsilon_{\text{H}} < 0$ because this would also cause $u_1$ to be positive such that $\rho_{\text{c}} < 0$. Nevertheless, an ordered antiferromagnetic phase has been reported for a 3D Heisenberg fluid with a negative coupling constant by Lomba *et al.* some time ago [37]. The formation of such an antiferromagnetic phase would only be signaled by the nematic-order parameter $\alpha_2$, whereas, $\alpha_1$, on which we concentrate here, vanishes even in such an ordered phase [37]. However, in the presence of the Heisenberg contribution, the dipolar contribution to $\varphi_{\text{anis}}$ may have an impact on the location of the critical line. This follows from the term in parentheses in Eq. (3.33).

Finally, it seems instructive to consider the predictions of a simple mean-field (SMF) approach. The latter is characterized by setting in Eq. (3.1),

$$g(\boldsymbol{r}_{12},\omega_1,\omega_2;\lambda) = \begin{cases} 0, & r_{12} < \sigma, \\ 1, & r_{12} \geqslant \sigma. \end{cases} \tag{3.36}$$

It is then relatively straightforward to demonstrate that the calculation of $\Delta\mathcal{F}$ gives an expression similar to the one presented in Eq. (3.25) where, however, $u_1$ has to be replaced by $\widetilde{u}_1$, defined by

$$\widetilde{u}_1 \equiv \frac{8\pi}{3}\beta_{\text{B}}\varepsilon_{\text{H}}\int_{\sigma}^{\infty} dr_{12} r_{12}^2 \varphi_{\text{att}}(r_{12}) = -\frac{32\pi}{9}\beta_{\text{B}}\varepsilon\varepsilon_{\text{H}}\sigma^3. \tag{3.37}$$

Hence, in Eq. (3.26), replacing $u_1$ by $\widetilde{u}_1$ leads to the simple analytic expression,

$$\beta_{\text{B}}^{\text{c}}\varepsilon\rho_{\text{c}}\sigma^3 = \frac{3}{16\pi}\frac{1}{\varepsilon_{\text{H}}} \tag{3.38}$$

for the line of IP phase transitions at the SMF level where $\beta_{\text{B}}^{\text{c}}$ is defined analogously to $\beta_{\text{B}}$ replacing, however, $T$ by the critical temperature $T_{\text{c}}$. A comparison between Eq. (3.38) and the more complex expression, resulting from Eqs. (3.26), (3.33), and (3.34) at the MMF level shows that, within the SMF approach, the dipolar contribution to $\varphi_{\text{anis}}$ is totally irrelevant for IP phase transitions. In fact, as seen from Eq. (3.33), it is only the cubic term in the expansion of the Boltzmann factor [see Eq. (3.29)] which yields a nonvanishing contribution of the dipolar term to the critical density. This justifies *a posteriori* our truncation of the power series in Eq. (3.29) after the term proportional to $\beta_{\text{B}}^3$.

## IV. ASPECTS OF FINITE-SIZE SCALING

To characterize the IP phase transition quantitatively, we introduce order parameters,

$$m_l = \int_{-1}^{1} dx\, \overline{\alpha}(x) P_l(x) = \frac{2}{2l+1}\alpha_l \tag{4.1}$$

based upon Eq. (3.8) where we employed the orthogonality relation (see Eq. (A9.b) of Ref. [43]) satisfied by the Legendre polynomials. Because, in the isotropic phase, $\overline{\alpha}(x) = \frac{1}{2}$ and because

$$\int_{-1}^{1} dx\, P_l(x) = 0, \quad \forall\, l \geqslant 1, \tag{4.2}$$

it follows that $m_l = 0$ in the isotropic phase for all $l \geqslant 1$. On the contrary, $m_l \neq 0$ if the system is in the polar phase. Because we have limited our discussion of the critical line of IP phase transitions to the leading terms in Eqs. (3.21) and (3.24) proportional to $\alpha_1$ [see also Eqs. (3.22)–(3.25)], we restrict the following discussion to $m_1$ as the order parameter, characterizing the IP phase transition.

One could determine $m_1$ within the scope of our MMF treatment as shown in detail by Groh and Dietrich [16] for pure fluids and as shown later by Range and Klapp [25] for binary mixtures of systems in which molecules are carrying an electrostatic point dipole. However, here, our goal is to employ a first-principles method, such as MC simulations to test the predictions and, therefore, the validity of the MMF theory developed in Secs. III A and III B. Consequently, we need an operational definition of $m_1$ suitable for computation in MC. To that end, we introduce the *instantaneous* order parameter,

$$m_1 \equiv \frac{1}{N}\left|\sum_{i=1}^{N} \widehat{\boldsymbol{u}}(\omega_i)\cdot\widehat{\boldsymbol{n}}\right|, \tag{4.3}$$

where $N$ denotes the number of molecules and the magnitude must be taken for reasons explained by Deutsch [49]. Following standard practice [5,6,11,47,50–52], we compute the director $\widehat{\boldsymbol{n}}$ as the eigenvector associated with the largest eigenvalue of the real, symmetric, and traceless alignment tensor,

$$\mathbf{Q} \equiv \frac{1}{2N}\sum_{i=1}^{N}[3\widehat{\boldsymbol{u}}(\omega_i)\otimes\widehat{\boldsymbol{u}}(\omega_i) - \mathbf{1}], \tag{4.4}$$

where the operator $\otimes$ represents the tensor product and $\mathbf{1}$ is the unit tensor. Numerically, we obtain $\widehat{\boldsymbol{n}}$ by applying Jacobi's method [53] to diagonalize $\mathbf{Q}$.

The ensemble average $\langle m_1\rangle$ should vanish in the isotropic phase according to the definition of $m_1$ given in Eq. (4.3). However, $\langle m_1\rangle = 0$ only in the thermodynamic limit. In any system of finite extent, $\langle m_1\rangle$ decays towards this limiting value in proportion to $1/\sqrt{N}$ (see Appendix A of Ref. [3]).

Therefore, in any system of finite extent, $\langle m_1\rangle > 0$ in the isotropic phase. The reason is that regions exist in which molecules align themselves in a *locally* parallel fashion because $\varphi_{\text{anis}}$ favors such an alignment [see Eqs. (2.4) and (2.5)] if the coupling constants $\varepsilon_{\text{H}}$ and $\varepsilon_{\text{D}}$ are chosen sensibly (see Sec. III D). Because, in the isotropic phase, no correlation between different locally ordered regions exists—provided their separation is larger than the range of $\varphi_{\text{anis}}$—an average over all the preferentially ordered but differently oriented domains in an *infinitely* large system would then give $\langle m_1\rangle = 0$. On the contrary, in a *finite* system, the different orientations of molecules in different uncorrelated domains of the system do not completely average out so that the actual value of $\langle m_1\rangle$ is the larger the smaller the system is according to its decay in proportion to $1/\sqrt{N}$ already mentioned above.

In an ideal ordered (polar) phase, $\langle m_1\rangle = 1$ because all molecules align themselves perfectly with $\widehat{\boldsymbol{n}}$ such that $\widehat{\boldsymbol{u}}(\omega_i)\cdot\widehat{\boldsymbol{n}} = 1$ for $i = 1,\ldots,N$. A preferred alignment of the molecules with $\widehat{\boldsymbol{n}}$ exists even if the ordered phase is nonideal ($\langle m_1\rangle < 1$). This causes finite-size effects to vanish sufficiently deep in the ordered phase (i.e., at sufficiently low $T$ or sufficiently high pressure $P$). In general, the variation in $\langle m_1\rangle$ with $T$ (or $P$) across the IP phase transition is weaker the lower $N$ is. Consequently, the variation in $\langle m_1\rangle$ in the vicinity of the IP phase transition is smeared out the smaller $N$ is.

To gain more detailed insight into such finite-size effects, it is useful to investigate the order-parameter distribution $\mathcal{P}(m_1)$ through its moments [54],

$$\langle m_1^k\rangle \equiv \int_0^1 dm_1 m_1^k \mathcal{P}(m_1). \tag{4.5}$$

To account quantitatively for the effects of finite system size, we make an *ansatz* and introduce a system-size-dependent analog of $\mathcal{P}(m_1)$ via [49]

$$\begin{aligned}\mathcal{P}_N(m_1) &= \mathcal{P}[m_1(N),t(N),N]\\ &\equiv N^{\beta/3\nu}\widetilde{\mathcal{P}}(N^{\beta/3\nu}m_1, N^{1/3\nu}t),\end{aligned} \tag{4.6}$$

where $t \equiv T/T_{\text{c}} - 1$ is a measure of distance from the critical temperature $T_{\text{c}}$ at the IP phase transition.

In Eq. (4.6) and below, tildes are used to refer to system-size-independent (rescaled) quantities. In the expression on the second line of Eq. (4.6), $\beta$ and $\nu$ are critical exponents, governing the growth of $\langle m_1\rangle$ and that of the correlation length in the vicinity of a critical point, respectively. The *ansatz* in Eq. (4.6) is valid if one assumes hyperscaling to be valid as well, that is, for a three-dimensional system, the relation,

$$3\nu - 2\beta - \gamma = 0 \tag{4.7}$$

is assumed to hold, which implies that, besides the correlation length, there is no other length diverging as $t = 0$ is approached [55]. In Eq. (4.7), $\gamma$ is the critical exponent, governing the divergence of the order-parameter susceptibility. Traditionally, one would make this *ansatz* by taking the linear extent $L$ of the system as the scaling variable rather than $N$. However, throughout this paper, we replace $L$ by $N^{1/3}$ because $N$ remains fixed in the MC simulations that we carry out in the isothermal-isobaric ensemble. In this ensemble, $L$ fluctuates around some average value $\langle L\rangle$ as the simulations progress, which makes the use of this variable in finite-size scaling approaches somewhat awkward.

Next, we introduce scaling functions $\widetilde{m}^{(k)}(N^{1/3\nu}t)$. This is accomplished by approximating $\mathcal{P}$ in Eq. (4.5) by its system-size-dependent counterpart $\mathcal{P}_N$ given in Eq. (4.6). Introducing $\widetilde{m}_1 \equiv N^{\beta/3\nu}m_1$ as a new integration variable and $\widetilde{t} \equiv N^{1/3\nu}t$,

$$\widetilde{m}^{(k)}(\widetilde{t}) \equiv N^{k\beta/3\nu}\int d\widetilde{m}_1 \widetilde{m}_1^k \widetilde{\mathcal{P}}(\widetilde{m}_1,\widetilde{t}) \tag{4.8}$$

follows without further ado. Equation (4.8) permits us to express the moments of the order-parameter distribution in Eq. (4.5) in terms of their scaling functions via

$$\langle m_1^k\rangle_N = N^{-k\beta/3\nu}\widetilde{m}^{(k)}(\widetilde{t}). \tag{4.9}$$

To locate the IP phase transition, we begin by first determining the critical temperature $T_{\text{c}}$. This can be accomplished by considering the second-order Binder cumulant defined as [49]

$$g_2(\widetilde{t}) \equiv \frac{\langle m_1^2\rangle_N}{\langle m_1\rangle_N^2} = \frac{\widetilde{m}^{(2)}(\widetilde{t})}{[\widetilde{m}^{(1)}(\widetilde{t})]^2}, \tag{4.10}$$

where the far right side follows with the aid of Eq. (4.9) and $\widetilde{t} = N^{1/3\nu}(T/T_{\text{c}} - 1)$. If plotted as a function of $T$ instead of the rescaled temperature $\widetilde{t}$, $g_2(T)$ for different $N$'s intersect in a unique point, which allows us to determine $T_{\text{c}}$ without any *a priori* knowledge of critical exponents. The value of $g_2(T)$ at $T = T_{\text{c}}$ is model dependent. The uniqueness of $g_2(T_{\text{c}})$ is a direct consequence of the system-size independence of the scaling functions at $T = T_{\text{c}}$. Moreover, if plotted as a function of $\widetilde{t}$, cumulants for different system sizes are expected to collapse onto a unique master curve in the near-critical regime where the scaling *ansatz* presented in Eq. (4.6) is valid [see Fig. 1(b)]. As demonstrated elsewhere [4], our model pertains to the universality class of the classical three-dimensional Heisenberg fluid characterized by $\beta = 0.3689(3)$, $\gamma = 0.7112(5)$, and $\nu = 1.3960(9)$ [7].

## V. RESULTS

### A. Numerical details

Results presented in this paper have been obtained by MC simulations in the isothermal-isobaric ensemble as discussed in greater detail in Ref. [3]. In this ensemble, a thermodynamic state is uniquely specified by the number of molecules $N$, pressure $P$, and temperature $T$. Employing a METROPOLIS algorithm adapted to the isothermal-isobaric ensemble as described in the book of Allen and Tildesley [56], we generate a Markov chain of configurations with a limiting distribution in configuration space proportional to $\exp\{-\beta_{\text{B}}[\Phi(\boldsymbol{R},\boldsymbol{\Omega}) + PV] + N\ \ln\ V\}$, where $V$ is the volume of the computational cell. To achieve this goal, one has to perform random displacements of the centers of mass of the molecules and their random rotation. Both substeps are attempted with equal probability where the specific molecule is picked sequentially. The $N$ attempts to either displace or rotate a molecule are followed by one attempt to change $V$. This is effected by rescaling the side lengths of the simulation box homogeneously (see p. 6 of Ref. [3]). Together, the $N$ translational and rotational and the single volume-change

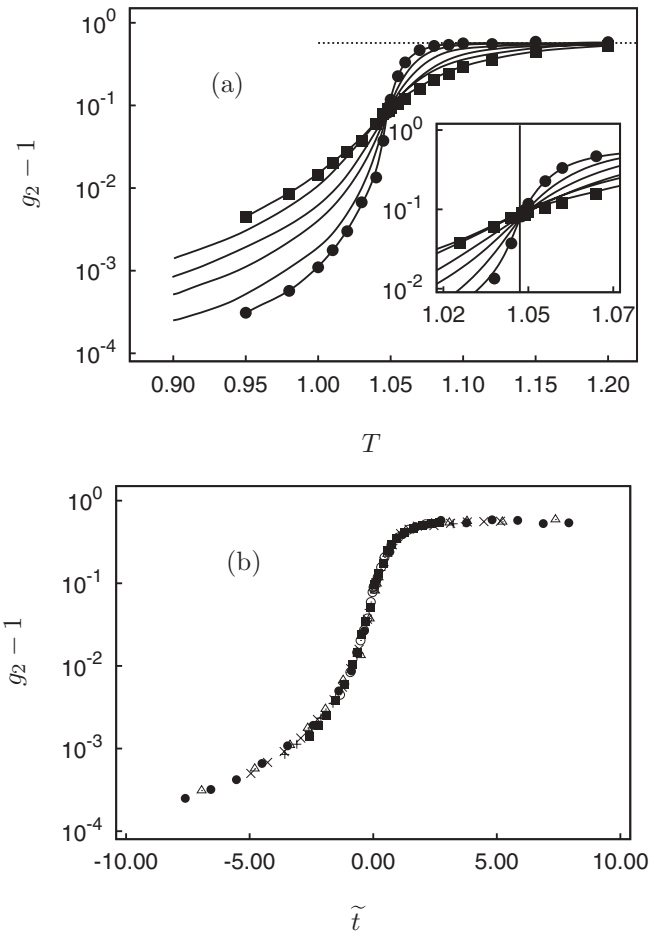


FIG. 1. (a) Plots of $g_2 - 1$ as functions of $T$ on a semilogarithmic scale for system sizes (•): $N = 300$ and (▲): $N = 10\,000$. The dashed horizontal line represents the limiting value of $g_2 - 1 = \frac{\pi}{2} - 1$ in the isotropic phase (see Ref. [3]). Intermediate curves are obtained for $N = 500$, $N = 1000$, $N = 2000$, and $N = 5000$. The inset is an enlargement of the plots around the transition temperature $T_{\rm IP} \simeq 1.047$ marked by the solid vertical line. (b) Data plotted in (a) collapse onto a master curve if plotted as functions of $\widetilde{t}$; (○): $N = 300$; (■): $N = 500$; (+): $N = 1000$; (×): $N = 2000$; (●): $N = 5000$; (△): $N = 10\,000$. Data have been obtained for $\varepsilon_{\rm H} = 0.06$, $\varepsilon_{\rm D} = 0.03$, and $P = 1.30$.

attempts constitute a MC cycle. Our runs are typically based upon $2 \times 10^4$ equilibration cycles followed by 2–4 $\times 10^5$ production cycles during which relevant ensemble averages are computed. In the immediate vicinity of the IP phase transition, the number of cycles are enlarged to $10^6$ cycles in a few test cases to make sure that our data are not plagued by critical slowing down. We consider system sizes ranging from $300 \leqslant N \leqslant 10\,000$.

In this paper, all quantities are expressed in terms of the customary reduced units. Length is given in units of $\sigma$, energy in units of $\varepsilon$, and temperature in units of $\varepsilon/k_{\rm B}$. Other derived quantities are expressed in terms of suitable combinations of these basic quantities. For example, pressure is given in units of $\varepsilon/\sigma^3$. Finally, unlike in our previous paper [3], we consider only a single pressure $P = 1.30$ but various values of the coupling constants $\varepsilon_{\rm H}$ and $\varepsilon_{\rm D}$.

### B. Cumulant analysis

To demonstrate the reliability of our numerical analysis, we begin with a discussion of the second-order Binder cumulant to locate the temperature at which the IP phase transition takes place. These results are obtained for $\varepsilon_{\rm H} = 0.06$ and $\varepsilon_{\rm D} = 0.03$. The choice of $\varepsilon_{\rm D} < 0$ in our earlier papers [3,4] was motivated because it offers molecules the possibility to form micelles and lamellae, which are often observed in amphiphilic suspensions. However, as we demonstrate, shortly, below, the actual sign of $\varepsilon_{\rm D}$ is inconsequential for the location of the IP phase transition.

Plots in Fig. 1(a) for the pressure $P = 1.30$ show that $g_2 - 1$ approaches the limiting value of $\frac{\pi}{2} - 1$ in the temperature range of thermodynamically stable isotropic phases and sufficiently far above $T_{\rm c}$, which is a consequence of the Gaussian nature of $\mathcal{P}(m_1)$ [3]. As $T$ decreases, $g_2 - 1$ decreases too. The onset of the departure from the limiting value of $\frac{\pi}{2} - 1$ begins at higher $T$ the smaller $N$ is. Eventually, at $T = T_{\rm c}$, all cumulants intersect in a unique point as expected for a continuous phase transition. With decreasing $T$, $g_2 - 1$ approaches zero in the polar phase. This is a consequence of the fact that, with increasingly lower $T$, $\mathcal{P}(m_1) \to \delta(m_1 - \langle m_1 \rangle)$ ($\delta$ denotes the Dirac $\delta$ function) because fluctuations of the order parameter around its average value are more and more suppressed [3]. The decrease in $g_2 - 1$ towards zero turns out to be more pronounced the larger $N$ is. Hence, the order of curves for various system sizes in Fig. 1(a) is inverted for $T < T_{\rm c}$ in the polar phase compared with the isotropic phase in the range of $T > T_{\rm c}$.

From the intersection of the curves in the inset of Fig. 1(a), we determine the critical temperature $T_{\rm c} \simeq 1.047$ of the IP phase transition. According to the arguments at the end of Sec. IV, one expects the data plotted in Fig. 1(a) to collapse onto a unique master curve if $T$ is replaced by $\widetilde{t}$ provided the value of $T_{\rm c}$ is sufficiently accurate and one knows the value of the critical exponent $\nu$. Plots in Fig. 1(b) show that, indeed, our data can be represented by the expected master curve over the entire temperature range considered. This clearly illustrates that our estimate of both $T_{\rm c}$ and $\nu$ is sufficiently accurate. Moreover, the results presented in Fig. 1(b) also indicate that our scaling *ansatz* in Eq. (4.6) is reliable for the range of system sizes considered in this paper such that, apparently, corrections to the simple scaling employed here are negligibly small.

### C. Monte Carlo simulations and modified mean-field theory

After demonstrating the reliability of the cumulant analysis, we are now turning to a systematic investigation of the influence of the coupling parameters $\varepsilon_{\rm H}$ and $\varepsilon_{\rm D}$ on the IP phase transition. As we demonstrated by plots in Figs. 1(a) and 1(b), the accuracy and resolution of our data permit a determination of the critical temperature $T_{\rm c}$ with sufficiently high precision. To save computer time, the following results are based upon data for only two system sizes $N = 1000$ and $N = 2000$ used in the cumulant analysis. To test the theoretical predictions derived in Sec. III B, it will be convenient to analyze the product $\beta_{\rm B}^{\rm c}\rho_{\rm c}$ [see, for example, Eq. (3.38)]. We determine $\rho_{\rm c}$ from plots of $\rho$ versus $T$ and linear interpolation over the temperature interval defined by the two data points immediately below and above $T_{\rm c}$. Plots in Fig. 2 reveal that this linear interpolation to find $\rho_{\rm c}$ can be expected to be reliable

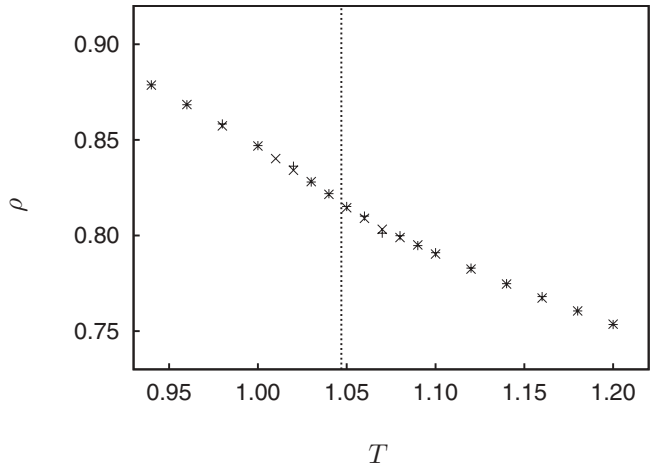


FIG. 2. Plots of $\rho$ as a function of $T$ for (+): $N = 1000$ and (×): $N = 2000$. The vertical dashed line demarcates the critical temperature $T_c \simeq 1.047$ determined from plots in Fig. 1(a).

because $\rho$ depends sufficiently weakly on $T$ and because there is no significant system-size effect. From Fig. 2, one also notices that the slope of the curves differs between regimes $T < T_c$ and $T > T_c$. This reflects a change in the thermal expansion coefficient $\alpha_P \equiv -\rho^{-1}(\partial\rho/\partial T)_P$, which passes through a maximum at $T \simeq T_c$. Intuitively, this makes sense because, as a response function, $\alpha_P$ is related to energy-density fluctuations [57], which are expected to become maximum at the (continuous) IP phase transition.

In Fig. 3, we present plots of $\beta_B^c\rho_c$ as a function of $1/\varepsilon_H$ obtained from a sequence of MC simulations. This plot is motivated by Eq. (3.38) obtained at the SMF level. As one can see, $\beta_B^c\rho_c$ increases with decreasing strength of the Heisenberg coupling constant in a slightly nonlinear fashion. Also shown in the figure is the prediction of the SMF theory represented by Eq. (3.38). The comparison reveals that the latter expression overestimates $\beta_B^c\rho_c$ increasingly as $1/\varepsilon_H$ becomes larger. On

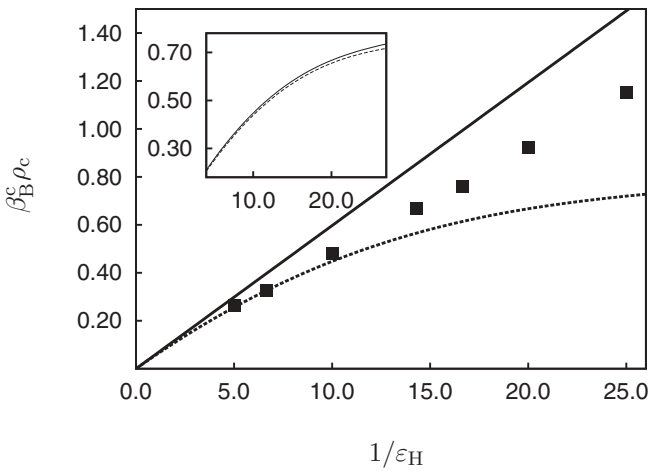


FIG. 3. Plots of $\beta_B^c\rho_c$ as a function of $1/\varepsilon_H$; (■): MC data; (–): from Eq. (3.38); (- - -): from Eq. (5.1). The inset is an enlargement where (–) is computed from Eqs. (3.34) and (5.1) and (- - -) is obtained from Eqs. (3.26), (3.33), and (3.34). All data sets are obtained for $\varepsilon_D = 0.03$.

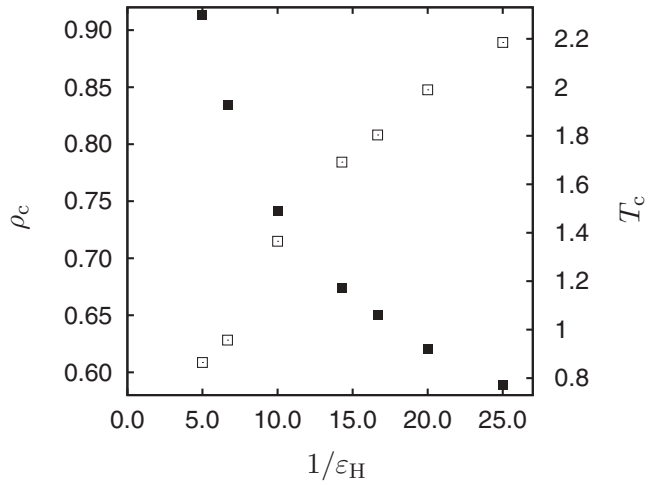


FIG. 4. Left ordinate (□): plots of $\rho_c$ and right ordinate (■): $T_c$ as functions of $1/\varepsilon_H$ obtained from MC at $\varepsilon_D = 0.03$.

the contrary, an improved representation of $\beta_B^c\rho_c$ is given when we use Eq. (3.33) but neglect the term proportional to $\beta_B^3$ [see Eq. (5.1)]. Using that truncation, from Fig. 3, we see that the MMF theory becomes nearly quantitative over the range of $5.0 \leqslant 1/\varepsilon_H \leqslant 10.0$. However, for weaker-coupling constants (i.e., at larger values of $1/\varepsilon_H$), the MMF treatment also fails increasingly to represent the simulation data adequately and underestimates $\beta_B^c\rho_c$ the more the larger $1/\varepsilon_H$ becomes.

The MMF results shown in Fig. 3 are obtained by neglecting, in the expression for $u_1$ in Eq. (3.33), the term proportional to $\beta_B^3$. From Eqs. (3.26) and (3.33), it is then easy to verify that [$\mathcal{I}^{(1)} < 0$, see Eqs. (2.3) and (3.34)]

$$\beta_B^c\rho_c \simeq -\frac{1}{4\pi\mathcal{I}^{(1)}}\frac{1}{\varepsilon_H}, \tag{5.1}$$

from which it is apparent that the overestimation of $\mathcal{I}^{(1)}$ at lower values of the Heisenberg coupling constant causes the leveling off of the MMF prediction for $\beta_B^c\rho_c$ as $1/\varepsilon_H$ increases. As one can see from the inset in Fig. 3, in the expression for $u_1$, incorporating the term proportional to $\beta_B^3$ [see Eq. (3.33)] is almost negligible except for the largest values of $1/\varepsilon_H$. The inset also indicates that, in the expression for $u_1$, incorporating the term proportional to $\beta_B^3$ deteriorates the agreement between our MMF theory and the MC results, but, only marginally. Nevertheless, it is pleasing to notice that the SMF theory and the MMF predictions give upper and lower bounds for the values of $\beta_B^c\rho_c$, respectively.

To unravel the origin of the less satisfactory description of our MC data by the MMF treatment in the low-coupling regime, in Fig. 4, we present separate plots of $\rho_c$ and $T_c$ for various values of $1/\varepsilon_H$. The plots in Fig. 4 clearly indicate that, with increasing $1/\varepsilon_H$, $\rho_c$ increases markedly, whereas, $T_c$ decreases steadily. This implies that our *ansatz* for the pair correlation function in Eq. (3.3) is less applicable as the coupling of the Heisenberg term in $\varphi_{anis}$ [see Eqs. (2.4) and (2.5)] becomes weaker (i.e., as $1/\varepsilon_H$ increases).

Next, it seems interesting to check the relative importance of the dipolar contribution to $\varphi_{anis}$. The MMF treatment detailed in Sec. III A suggests that the dipolar contribution to the critical line $\rho_c(T_c)$ is subdominant to the Heisenberg one for

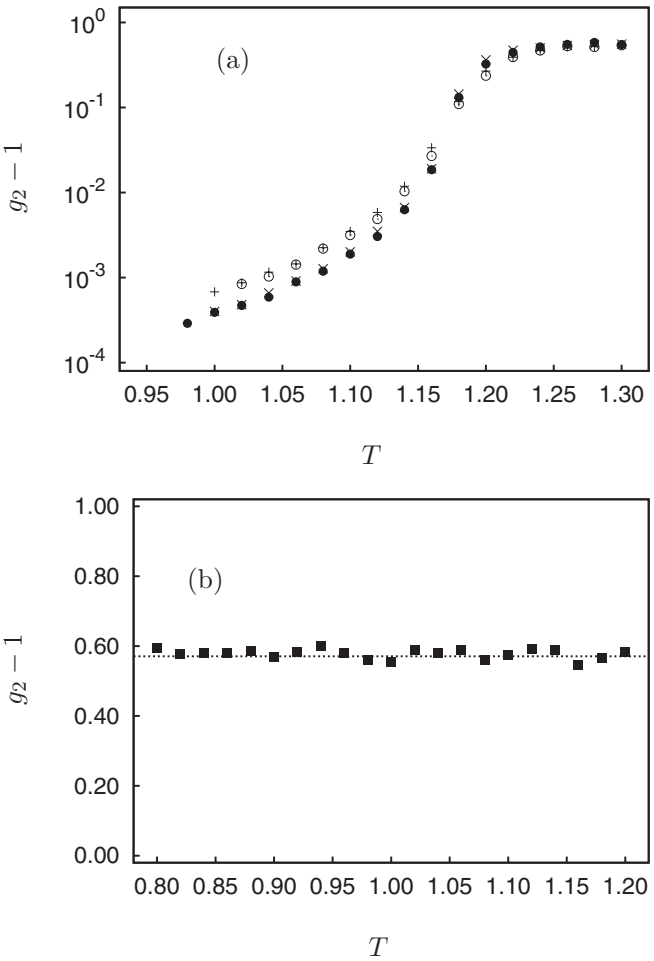


FIG. 5. Plots of $g_2 - 1$ as functions of $T$. (a) $\varepsilon_D = 0.03$, (○): $N = 1000$, and (●) $N = 2000$; $\varepsilon_D = -0.03$, (×): $N = 1000$, and (+): $N = 2000$. In all cases, $\varepsilon_H = 0.07$. (b) as (a) but for $\varepsilon_H = 0.00$ and $\varepsilon_D = 0.03$. The dashed line represents the limiting value $g_2 - 1 = \frac{\pi}{2} - 1$ in the isotropic phase [4].

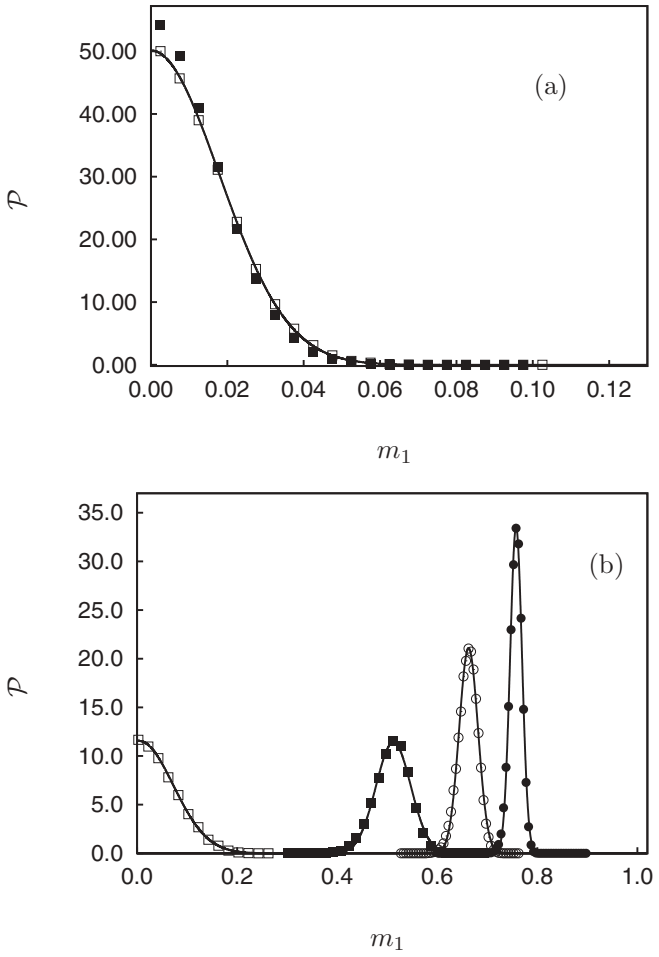


FIG. 6. (a) Plots of $\mathcal{P}(m_1)$ for $N = 1000$. (a) $\varepsilon_H = 0.00$, $\varepsilon_D = 0.03$; (□): $T = 1.20$; and (■): $T = 0.80$. (b) as (a) but for $\varepsilon_H = 0.07$, $\varepsilon_D = 0.03$; (□): $T = 1.30$; (■): $T = 1.12$; (○): $T = 1.02$; and (●): $T = 0.90$ [see also Fig. 5(a)]. The solid lines in parts (a) and (b) of the figure are fits of a Gaussian to the discrete MC data sets.

coupling constants less than 1 because $\varepsilon_D$ enters Eq. (3.33) quadratically in lowest order, whereas, the expression in Eq. (3.33) depends linearly on $\varepsilon_H$ [see also Eq. (3.26)]. Plots in Fig. 5(a) show that, for a nonvanishing coupling constant of the Heisenberg contribution to $\varphi_{anis}$ [see Eqs. (2.4) and (2.5)], an IP phase transition occurs signaled by the intersection of the second-order cumulants for the two different particle numbers. However, the sign of the dipolar coupling constant is apparently irrelevant for this transition indicated by the fact that the curves for the same $N$ and $\varepsilon_D > 0$ can be superimposed to those for $\varepsilon_D < 0$ within statistical errors of the simulation data. Because the sign of $\varepsilon_D$ becomes relevant only through the last term in parentheses in Eq. (3.33) and because this term is proportional to $\varepsilon_D^3$, the impact of whether $\varepsilon_D$ is positive or negative is expected to have only a negligible influence on the location of the IP phase transition given the magnitude of the coupling constants in Fig. 5. Hence, our data plotted in Fig. 5(a) comport with the theoretical predictions.

Moreover, the plot in Fig. 5(b) illustrates that, in the case of a vanishing Heisenberg coupling constant, the IP phase transition vanishes, too. This is reflected by the fact that, for $\varepsilon_H = 0.00$, $g_2 - 1$ turns out to be temperature independent and fluctuates around its limiting value of $\frac{\pi}{2} - 1$ over a range of $T$ where the corresponding plots in Fig. 5(a) exhibit clear evidence for an IP phase transition. The limiting value can be rationalized by assuming that the order-parameter distribution is Gaussian in the isotropic phase centered on $m_1 = 0$. It is then easy to verify that $\langle |m_1| \rangle = \sqrt{2\sigma_{\mathcal{P}}^2/\pi}$, whereas, $\langle m_1^2 \rangle = \sigma_{\mathcal{P}}^2$ such that $g_2 = \frac{\pi}{2}$ follows from Eq. (4.10) without further ado. For $T < 0.8$, the system characterized by $\varepsilon_H = 0.00$ and $\varepsilon_D = 0.03$ seems to enter a solidlike or glassy state as we inferred from an inspection of snapshots of individual configurations generated in the MC simulations. This suggests solidification rather than formation of a polar liquidlike phase in the absence of the Heisenberg contribution to $\varphi_{anis}$ in Eq. (2.4).

That the order-parameter distribution in the isotropic phase is, indeed, Gaussian as surmised above is illustrated by plots in Fig. 6(a). Notice that, in both plots presented in Fig. 6(a), $\langle |m_1| \rangle = 0$. Hence, the Gaussian order-parameter distribution is solely governed by $\sigma_{\mathcal{P}}$ such that the slight deviation in peak height and width between the two distributions plotted in Fig. 6(a) reflects the scatter of the corresponding data

points plotted in Fig. 5(b). For a nonvanishing Heisenberg coupling constant, plots in Figs. 5(a) reflect the existence of an IP phase transition. Consequently, the order-parameter distribution shifts to larger values of $\langle|m_1|\rangle$ with decreasing $T$ as one can see from the plots in Fig. 6(b). However, with lower $T$, $\mathcal{P}(m_1)$ becomes both taller and narrower such that, in the limit of vanishing $T$,

$$\lim_{T\to 0} \mathcal{P}(m_1) = \delta(m_1 - \langle|m_1|\rangle). \tag{5.2}$$

Thus, it follows from Eq. (4.5) that, in the limit of vanishing temperature, $\langle m_1^2\rangle = \langle|m_1|\rangle^2$, which reflects the vanishing of order-parameter fluctuations in that limit (i.e., a vanishing order-parameter susceptibility). This also implies $\lim_{T\to 0}(g_2 - 1) = 0$ in agreement with MC data plotted in Figs. 1 and 5(a).

## VI. SUMMARY AND CONCLUSIONS

In this paper, we investigate the IP phase transition in an anisometric Lennard-Jones fluid by means of mean-field DFT and MC simulations in the isothermal-isobaric ensemble. In these simulations, we locate the critical temperature at the IP phase transition by analyzing the second-order Binder cumulant of the dipolar-order parameter for various system sizes. Once $T_c$ has been determined, $\rho_c$ can be calculated from the temperature dependence of the mean density also accessible in the MC simulations.

Our numerical results show that both $T_c$ and $\rho_c$ depend on the coupling strength $\varepsilon_H$ of the Heisenberg contribution to the anisotropic part of our intermolecular interaction potential. On the contrary, the dipolelike (yet short-ranged) contribution turns out to be largely irrelevant for the IP phase transition in the range of coupling constants for which the system in parallel MC simulations is still fluidlike. We interpret this feature as a consequence of the short-range character of the interaction. Indeed, for true long-range dipolar interactions, the formation of ordered phases is determined by the magnitude of the dipole moment, which is the analog of $\sqrt{\varepsilon_D}$ in our model.

The insensitivity of the IP phase transition in our MC simulations is reflected by two features. First, for fixed $\varepsilon_H$, the sign of $\varepsilon_D$ does not matter. Second, for $\varepsilon_H = 0.00$, the IP phase transition is suppressed over the same temperature range over which it takes place for nonvanishing $\varepsilon_H$. Instead, we observe indications for solidification.

In the parallel theoretical treatment, our results are based upon two approximations made to the orientation-dependent pair correlation function. In the simplest version of the theory (SMF), correlations between a pair of molecules are neglected altogether for separations exceeding the hard-core diameter of the molecules. In this SMF treatment, the IP phase transition is solely driven by the Heisenberg contribution to the intermolecular interaction potential. The ratio of critical density $\rho_c$ to critical temperature $T_c$ at the IP phase transition is predicted to be inversely proportional to the Heisenberg coupling constant $\varepsilon_H$, which turns out to provide a sufficiently accurate description of the MC data in the strong-coupling limit, that is, as $1/\varepsilon_H$ vanishes.

In the more elaborate MMF treatment, we approximate the pair correlation function by its form in the limit of vanishing density. Together with a high-temperature expansion, we show that, in lowest order, $\beta_B^c\rho_c$ is also proportional to $1/\varepsilon_H$ but exhibits a weak temperature dependence unlike at the SMF level. Including higher-order terms in the high-temperature expansion of the pair correlation function, on which the MMF treatment is based, causes $\beta_B^c\rho_c$ to also depend on the dipolar contribution to the anisotropic part of the intermolecular interaction potential. Unfortunately, including higher-order terms deteriorates the agreement between DFT and MC results, but, only marginally. In the complete absence of the Heisenberg term (i.e., for $\varepsilon_H = 0.00$), the critical density predicted by the MMF theory turns out to be unphysical in cases where $\varepsilon_D$ is positive. Hence, polar phases cannot form if $\varphi_{anis}$ depends solely on the (short-range) dipolelike contribution to $\Psi$ consistent with earlier theoretical arguments.

Thus, both versions of the mean-field theory agree qualitatively with the numerical results in that an IP phase transition cannot occur in the absence of the Heisenberg contribution to the anisotropic part of the interaction potential. If the coupling constant of the Heisenberg contribution is sufficiently large, the MMF theory agrees semiquantitatively with the MC results. The range of coupling constants for which this is the case significantly exceeds the range over which the agreement with the SMF theory is satisfactory so that the MMF approach gives an improvement over the simple version of the mean-field theory. However, in developing the MMF theory for the present model, it turns out to suffice to consider only the linear term in $\beta_B$ in the high-temperature expansion of the Mayer $f$ function. Instead, the agreement between DFT and MC data is expected to become better if a more suitable approximation of the pair correlation function would be employed.

In the case of "antidipoles" (i.e., for $\varepsilon_D < 0$), the possibility for an IP phase transition exists *in principle* because one would obtain physically sensible values for the critical density $\rho_c$ from Eqs. (3.26) and (3.35). However, polar phases for antidipolar interactions cannot form because the anisotropic part of the interaction potential favors an antiparallel rather than a parallel orientation of a pair of nearest-neighbor molecules, which consequently destroys the possibility of forming polar phases even at low temperatures or high pressures.

## ACKNOWLEDGMENTS

Two of us (S.G. and M.S.) acknowledge financial support from *Deutsche Forschungsgemeinschaft* through Grant No. Scho 525-9. In addition, support from the International Graduate Research Training Group "Self-assembled soft matter nanostructures at interfaces" is gratefully acknowledged by S.H.L.K. and M.S.

[1] T. Erdmann, M. Kröger, and S. Hess, Phys. Rev. E **67**, 041209 (2003).

[2] M. Melle, M.S. thesis, Technische Universität Berlin, 2010.

[3] M. Melle, S. Giura, S. Schlotthauer, and M. Schoen, J. Phys.: Condens. Matter **24**, 035103 (2012).
[4] M. Melle, S. Giura, S. Schlotthauer, and M. Schoen, J. Phys.: Condens. Matter **24**, 209401 (2012).
[5] J. J. Weis, J. Chem. Phys. **123**, 044503 (2005).
[6] J. J. Weis and D. Levesque, J. Chem. Phys. **125**, 034504 (2006).
[7] M. Campostrini, M. Hasenbusch, A. Pelissetto, P. Rossi, and E. Vicari, Phys. Rev. B **65**, 144520 (2002).
[8] G. Ayton, M. J. P. Gingras, and G. N. Patey, Phys. Rev. Lett. **75**, 2360 (1995).
[9] G. Ayton, M. J. P. Gingras, and G. N. Patey, Phys. Rev. E **56**, 562 (1997).
[10] A. Perera and G. N. Patey, J. Chem. Phys. **91**, 3045 (1989).
[11] D. Wei and G. N. Patey, Phys. Rev. Lett. **68**, 2043 (1992).
[12] D. Wei and G. N. Patey, Phys. Rev. A **46**, 7783 (1992).
[13] D. Wei, G. N. Patey, and A. Perera, Phys. Rev. E **47**, 506 (1993).
[14] P. Frodl and S. Dietrich, Phys. Rev. A **45**, 7330 (1992).
[15] P. Frodl and S. Dietrich, Phys. Rev. E **48**, 3203 (1993).
[16] B. Groh and S. Dietrich, Phys. Rev. E **50**, 3814 (1994).
[17] B. Groh and S. Dietrich, Phys. Rev. E **54**, 1687 (1996).
[18] B. Groh and S. Dietrich, Phys. Rev. E **53**, 2509 (1996).
[19] B. Groh and S. Dietrich, Phys. Rev. Lett. **79**, 749 (1997).
[20] B. Groh and S. Dietrich, Phys. Rev. E **55**, 2892 (1997).
[21] S. Klapp and F. Forstmann, J. Chem. Phys. **106**, 9742 (1997).
[22] S. H. L. Klapp and G. N. Patey, J. Chem. Phys. **112**, 3832 (2000).
[23] S. Klapp and F. Forstmann, Europhys. Lett. **38**, 663 (1997).
[24] S. H. L. Klapp and G. N. Patey, J. Chem. Phys. **112**, 10949 (2000).
[25] G. M. Range and S. H. L. Klapp, Phys. Rev. E **69**, 041201 (2004).
[26] J. M. Tavares, M. M. Telo da Gama, P. I. C. Teixeira, J. J. Weis, and M. J. P. Nijmeijer, Phys. Rev. E **52**, 1915 (1995).
[27] C. Spöler and S. H. L. Klapp, J. Chem. Phys. **118**, 3628 (2003).
[28] M. Gramzow and S. H. L. Klapp, Phys. Rev. E **75**, 011605 (2007).
[29] J. M. Tavares, J. J. Weis, and M. M. Telo da Gama, Phys. Rev. E **73**, 041507 (2006).
[30] J. S. Høye and G. Stell, Phys. Rev. Lett. **36**, 1569 (1976).
[31] P. C. Hemmer and D. Imbro, Phys. Rev. A **16**, 380 (1977).
[32] L. Feijoo, C.-W. Woo, and V. T. Rajan, Phys. Rev. B **22**, 2404 (1980).
[33] R. M. Stratt, Phys. Rev. Lett. **53**, 1305 (1984).
[34] P. de Smedt, P. Nielaba, J. L. Lebowitz, J. Talbot, and L. Dooms, Phys. Rev. A **38**, 1381 (1988).
[35] D. Marx, P. Nielaba, and K. Binder, Phys. Rev. Lett. **67**, 3124 (1991).
[36] E. Lomba, J. J. Weis, N. G. Almarza, F. Bresme, and G. Stell, Phys. Rev. E **49**, 5169 (1994).
[37] E. Lomba, J. J. Weis, and G. Stell, Phys. Rev. E **50**, 3853 (1994).
[38] J. J. Weis, M. J. P. Nijmeijer, J. M. Tavares, and M. M. Telo da Gama, Phys. Rev. E **55**, 436 (1997).
[39] T. G. Sokolovska, Physica A **253**, 459 (1998).
[40] T. G. Sokolovska and R. O. Sokolovskii, Phys. Rev. E **59**, R3819 (1999).
[41] H. E. Stanley, *Introduction to Phase Transitions and Critical Phenomena* (Oxford University Press, Oxford, 1987), Chap. 8.
[42] W. Nolting, *Grundkurs Theoretische Physik*, (Springer-Verlag, Berlin, 2004), Vol. 3, Chap. 2.2.8.
[43] C. G. Gray and K. E. Gubbins, *Theory of Molecular Fluids* (Clarendon, Oxford, 1984), Vol. 1, Appendix A.
[44] R. Evans, Adv. Phys. **28**, 143 (1979).
[45] P. I. Teixeira and M. M. Telo da Gama, J. Phys.: Condens. Matter **3**, 111 (1991).
[46] N. F. Carnahan and K. E. Starling, J. Chem. Phys. **51**, 635 (1969).
[47] S. H. L. Klapp and M. Schoen, J. Chem. Phys. **117**, 8050 (2002).
[48] M. A. Osipov, P. I. C. Teixeira, and M. M. Telo da Gama, J. Phys. A **30**, 1953 (1997).
[49] H. P. Deutsch, J. Stat. Phys. **67**, 1039 (1992).
[50] R. Eppenga and D. Frenkel, Mol. Phys. **52**, 1303 (1992).
[51] M. Greschek, M. Melle, and M. Schoen, Soft Matter **6**, 1898 (2010).
[52] M. Greschek and M. Schoen, Phys. Rev. E **83**, 011704 (2011).
[53] W. Press, S. A. Teukolsky, W. T. Vetterling, and B. P. Flannery, *Numerical Recipes in FORTRAN* (Cambridge University Press, Cambridge, UK, 1989), Chap. 11.1.
[54] D. P. Landau and K. Binder, *A Guide to Monte Carlo Simulations in Statistical Physics* (Cambridge University Press, Cambridge, UK, 2005).
[55] K. Binder, *Finite Size Effects at Phase Transitions* (Springer-Verlag, Berlin, 1992).
[56] M. P. Allen and D. J. Tildesley, *Computer Simulation of Liquids* (Clarendon, Oxford, 1987).
[57] M. Schoen, Physica A **270**, 353 (1999).